ISIJ International, Vol. 46 (2006), No. 3, pp. 441–449

Crystallization of $CaO–SiO_2–TiO_2$ Slag as a Candidate for Fluorine Free Mold Flux

Hideko NAKADA and Kazuhiro NAGATA

Department of Chemistry and Materials Science, Tokyo Institute of Technology, 2-12-1, Ookayama, Meguro-ku, Tokyo 152-8552 Japan. hideko@mtl.titech.ac.jp

(*Received on July 19, 2005; accepted on October 28, 2005*)

The time-temperature-transformation diagram (TTT diagram) of $CaO–SiO_2–TiO_2$ slag has been determined by using differential thermal analysis (DTA) in order to investigate the crystallization of the slag as a candidate for fluorine free mold flux. The incubation time of $CaOSiO_2TiO_2$ in $CaO–SiO_2–TiO_2$ slag is as small as that of cuspidine ($3CaO_2SiO_2CaF_2$) in commercial mold fluxes. This finding indicates that the $CaOSiO_2TiO_2$ crystallizes rapidly in the slag film between the mold and the steel in the continuous casting machine, similar to cuspidine in commercial mold fluxes. $CaOSiO_2TiO_2$ in $CaO–SiO_2–TiO_2$ slag is substituted for cuspidine in commercial mold fluxes. The thickness of the crystalline layer of $CaOSiO_2TiO_2$ is smaller than that of cuspidine. In order to improve the heat transfer control of $CaO–SiO_2–TiO_2$ slag, it is necessary to decrease the incubation time of $CaOSiO_2TiO_2$ at high temperature.

KEY WORDS: heat transfer control; TTT diagram; $CaO–SiO_2–TiO_2$ slag; fluorine free mold flux.

1. Introduction

In the continuous casting of steel, mold flux which mainly consists of $CaO–SiO_2–CaF_2$ system has many functions. The important functions are (1) lubrication between the steel and the mold and (2) heat transfer control for decreasing of the heat flux from the steel to the mold in order to prevent longitudinal cracks on the steel surface.[1,2] The crystallization of cuspidine ($3CaO_2SiO_2CaF_2$) from mold flux is thought to be the most effective way for the heat transfer control. Although the mechanism of the heat transfer control by the crystallization of cuspidine has not been determined yet, two ideas for the mechanism have been proposed. One is that radiation heat flux is decreased by scattering at the boundary between the crystalline and the liquid layers[3–8] and the other is that total heat flux is decreased by the large thermal resistance of the air gap formed as a result of the solidification shrinkage.[5,9–15] Anyway, the crystallization of cuspidine from mold flux has the great effect on the heat transfer control.

However, fluorine which is a main component of cuspidine ($3CaO_2SiO_2CaF_2$) exerts the harmful influence on environment. Therefore, fluorine free mold flux has been strongly required. Any fluorine free mold flux has not been proposed yet. The roles of CaF_2 addition to commercial mold fluxes are to decrease the liquidus temperature and the viscosity in $CaO–SiO_2–CaF_2$ system[16,17] for the lubrication and to compose cuspidine for the heat transfer control, respectively. Resembling to the role of CaF_2, TiO_2 decreases the liquidus temperature and the viscosity in $CaO–SiO_2–TiO_2$ slag.[18,19] This tendency expects that $CaO–SiO_2–TiO_2$ slag has the same role of the lubrication as commercial mold fluxes. In order to propose $CaO–SiO_2–TiO_2$ slag as a candidate for fluorine free mold flux, it is required that $CaO–SiO_2–TiO_2$ slag has the heat transfer control function. It is necessary that the crystals of $CaO–SiO_2–TiO_2$ system precipitate like cuspidine in commercial mold fluxes. Therefore, it is essential to study the crystallization behavior of $CaO–SiO_2–TiO_2$ slag.

Figure 1 shows the microstructure of the crystalline layer of the commercial mold flux used in KOBE steel.[20] The crystalline layer of cuspidine takes dendrite and cubic structures. **Table 1** summarizes the microstructure of the crystalline layer in commercial mold fluxes.[11,20,21] Any commercial mold flux provides the crystalline layer of cuspidine as reported by Grievson *et al.*[22] The crystalline layer in the commercial mold fluxes also presents cubic structure

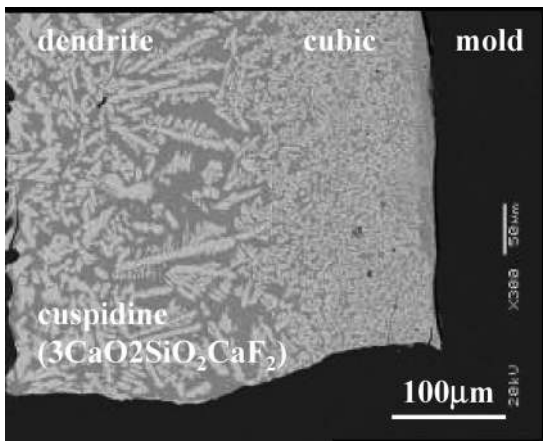

Fig. 1. Microstructure of the commercial mold flux on the mold side.[20]

© 2006 ISIJ

Table 1. Microstructure of the crystalline layer in commercial mold fluxes.

commercial mold fluxes	specification of mold flux			microstructure of cuspidine		
	CaO/SiO_2	crystallization temperature /K	category of steel	mold side → shell side		
				cubic	dendrite	gallasy
flux A[21)]	1.01	1496	hypo-peritectic	0-400μm	undetectable	400μm-1mm
flux B[21)]	1.15	1509	hypo-peritectic	0-300μm	300μm-900μm	900μm-1mm
flux C[11)]	1.42	1415	midium carbon	galassy	450μm-2.4mm	undetectable
flux D[11)]	1.47	1398	midium carbon	0-570μm	570μm-2mm	undetectable
flux E[11)]	1.46	1418	midium carbon	0-500μm	500μm-3.5mm	undetectable
flux F[20)]	0.91	1413	midium carbon	0-150μm	150μm-400μm	undetectable

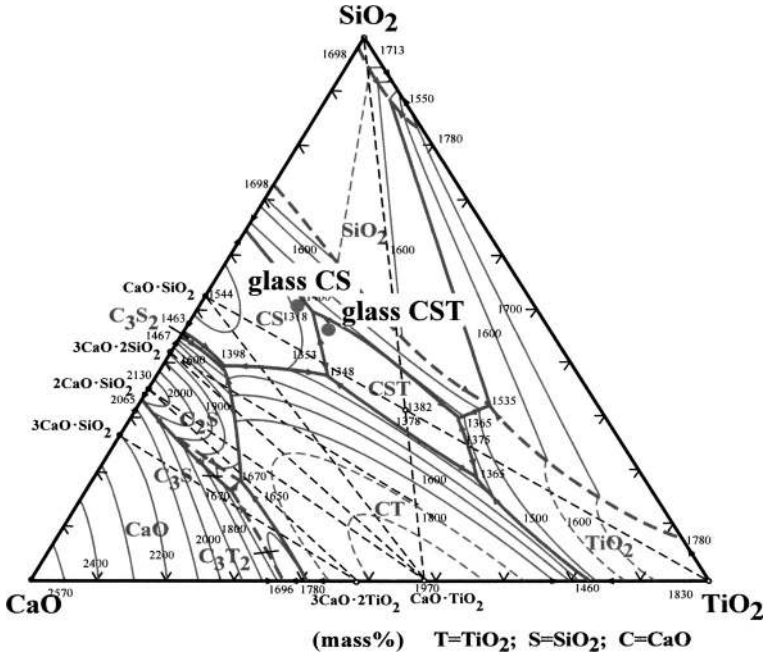

Fig. 2. Equilibrium phase diagram of $CaO–SiO_2–TiO_2$ system.

on the mold side with lower temperature and dendrite structure from middle to the shell side with higher temperature. It is considered that cuspidine with the dendrite structure crystallizes rapidly from liquid on the shell side and cuspidine with the cubic structure precipitates from once quenched glass on the mold side. As shown Table 1, although the amount of the dendrite and the cubic structures varies with each commercial mold flux, most of the crystalline layer takes the dendrite structure. This finding that cuspidine is able to crystallize from liquid rapidly as primary crystal. Actually, Hanao *et al.*[21)] reported that the rapid crystallization of cuspidine brings the great effect on the heat transfer control *i.e.* the crystallization of cuspidine from liquid as primary crystal brings the great effect on the heat transfer control. Thus, it is necessary that the crystallization rate of the crystals in $CaO–SiO_2–TiO_2$ slag is compared with that of cuspidine in commercial mold fluxes. The crystallization rate of the crystals is defined as the incubation time in the time-temperature-transformation diagram (TTT diagram) of $CaO–SiO_2–TiO_2$ slag.

The aim of this study is to investigate TTT diagram of $CaO–SiO_2–TiO_2$ slag and to examine whether $CaO–SiO_2–TiO_2$ slag is proposed as a candidate for fluorine free mold flux.

2. Experimental

2.1. Sample Preparation

Figure 2 shows the equilibrium phase diagram of $CaO–SiO_2–TiO_2$ system.[18)] In this study, two series of glassy sample were prepared. The samples of glass CST series with the basicity of 0.83 were prepared in the initial field of $CaOSiO_2TiO_2$ and the samples of glass CS series with the basicity of 0.84 were prepared in the initial field of $CaOSiO_2$. **Table 2** shows the chemical compositions of the samples. The compositions of the samples were selected from the reason that the liquidus temperature and the viscosity of the samples are similar to those of commercial mold fluxes in $CaO–SiO_2–CaF_2$ system. The samples of glass CST series have the same composition but have the different cooling rate of DTA varying from 0.183 to 2.36 K/s. In a similar way, the samples of glass CS series have the same composition but have the different cooling rate varying from 0.173 to 6.83 K/s. The composition of the samples was determined with accuracy using the quantitative analysis of electron probe micro analysis (EPMA). $CaOSiO_2TiO_2$ crystal was used as the standard material for the quantitative analysis. The samples were prepared from regent grade SiO_2, TiO_2 and $CaCO_3$ powders. $CaCO_3$ was decomposed into CaO at 1 273 K for 24 h. The mixtures of SiO_2, TiO_2 and CaO were melted in a platinum crucible at

© 2006 ISIJ

Table 2. Crystallization temperature and crystallization time of DTA measurement.

Sample series	Sample No.	chemical compositions (mol %)				melting point /K	cooling rate of DTA measurement /Ks^{-1}	Peak 1		Peak 2		Peak 3	
		CaO	SiO_2	TiO_2	CaO/SiO_2			crystallization time /s	crystallization temperature /K	crystallization time /s	crystallization temperature /K	crystallization time /s	crystallization temperature /K
glass CST	glass CST-A	37.43	45.32	17.25	0.83	1585	0.183	149	1557	175	1552	undetected	undetected
	glass CST-B	37.43	45.32	17.25	0.83	1585	0.373	undetected	undetected	153	1527	undetected	undetected
	glass CST-C	37.43	45.32	17.25	0.83	1585	1.94	undetected	undetected	65.7	1457	214	1167
	glass CST-D	37.43	45.32	17.25	0.83	1585	2.36	undetected	undetected	undetected	undetected	144	1236
glass CST	glass CS-A	40.15	47.79	12.05	0.84	1569	0.173	775	1423	913	1397	undetected	undetected
	glass CS-B	40.15	47.79	12.05	0.84	1569	0.600	297	1390	402	1326	675	1159
	glass CS-C	40.15	47.79	12.05	0.84	1569	0.633	284	1389	339	1354	562	1210
	glass CS-D	40.15	47.79	12.05	0.84	1569	0.800	197	1405	269	1345	436	1204
	glass CS-E	40.15	47.79	12.05	0.84	1569	0.917	196	1387	222	1362	372	1220
	glass CS-F	40.15	47.79	12.05	0.84	1569	1.18	undetected	undetected	189	1344	336	1167
	glass CS-G	40.15	47.79	12.05	0.84	1569	1.22	171	1360	192	1333	312	1185
	glass CS-H	40.15	47.79	12.05	0.84	1569	1.93	undetected	undetected	133	1311	211	1157
	glass CS-I	40.15	47.79	12.05	0.84	1569	2.72	undetected	undetected	98.5	1301	154	1158
	glass CS-J	40.15	47.79	12.05	0.84	1569	3.35	undetected	undetected	82.2	1294	127	1142
	glass CS-K	40.15	47.79	12.05	0.84	1569	5.70	undetected	undetected	54.8	1256	96.5	1022
	glass CS-L	40.15	47.79	12.05	0.84	1569	6.83	undetected	undetected	undetected	undetected	74.0	1085

1 723 K for 1 h in air and then quenched by sandwiching the melt with two copper blocks. In order to produce the glassy sample, the samples were identified to be amorphous by X-ray diffraction.

2.2. Measurement

The continuous-cooling-transformation diagram (CCT diagram) was experimentally determined by using differential thermal analysis (DTA) and was transformed into TTT diagram by using the additivity rule of Schiel.[23,24]

DTA measurement were carried out in order to decide the crystallization temperature and the crystallization time at each continuous cooling rate, as shown in Table 2. About 50 mg of ground glassy samples were enclosed into a Pt container fixed onto the thermocouple directly. Ground glassy samples were melted completely above the melting point for 5 min and the molten samples were cooled at the constant cooling rate in Ar gas flow of 50 mL/min. Exothermic peaks on the continuous cooling process indicates the crystallization from the molten samples. The temperature and the time at each exothermic peak were measured as the crystallization temperature and the crystallization time of the samples, respectively. Pure α-Al_2O_3 powder was selected as the reference material of DTA measurement. In order to correct the influence of the cooling rate and the Pt container, the measured crystallization temperature was calibrated by using the known melting points of CaF_2 and MgF_2.

X-ray diffraction studies were carried out by using Cu-Kα radiation and the crystals of the samples after DTA measurement were identified. The microstructure of the samples was observed by EPMA in order to identify the crystals of the samples and determine the sequence of the crystallization during the continuous cooling. The accelerator voltage of electron beam was 15 kV. Sample current image (SC image) and back scattered electron image (BSE image) of the samples were obtained. The characteristic X-ray images of Ca, Si, Ti and O were measured in order to identify the crystal of the samples and compared with the results of X-ray diffraction.

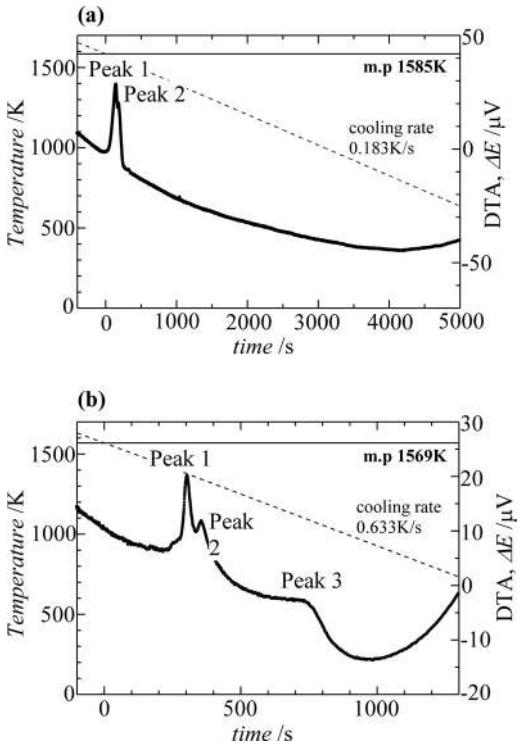

Fig. 3. DTA curve of (a) glass CST-A sample and (b) glass CS-C sample.

3. Results

3.1. CCT Diagram of Glass CST

3.1.1. Identification of Phases by DTA Measurement, X-ray Diffraction and EPMA for Glass CST

Figure 3(a) shows the DTA curve of glass CST-A sample whose cooling rate is 0.183 K/s. In glass CST-A sample, there are two exothermic peaks. The peak with higher temperature and the peak with lower temperature are named to be Peak 1 and Peak 2, respectively. In Table 2, the crystallization temperature and the crystallization time of the sam-

© 2006 ISIJ

ples are summarized. The melting points of the samples are determined by the heating process of DTA measurement. Three kinds of the exothermic peak, Peak 1–Peak 3, are detected. Peak 1 is detected only in glass CST-A sample and Peak 3 is detected in glass CST-C sample and glass CST-D sample.

Figure 4 shows the characteristic X-ray image of Ti for glass CST-B sample. Glassy phases and the phase which consists of the small grains of $CaOSiO_2TiO_2$ and $CaOSiO_2$ were observed. In **Table 3**, the crystals observed by EPMA are summarized. Glass CST-C sample with Peak 2 and Peak 3 in DTA data is composed of two phases of $CaOSiO_2TiO_2$ and glass. Glass CST-D sample with only Peak 3 has only glassy phase.

Figures 5(a) and 5(b) show the X-ray diffractions of glass CST-A sample and glass CST-C sample, respectively. In glass CST-A sample, $CaOSiO_2TiO_2$ and $CaOSiO_2$ are identified, while in glass CST-C sample only $CaOSiO_2TiO_2$

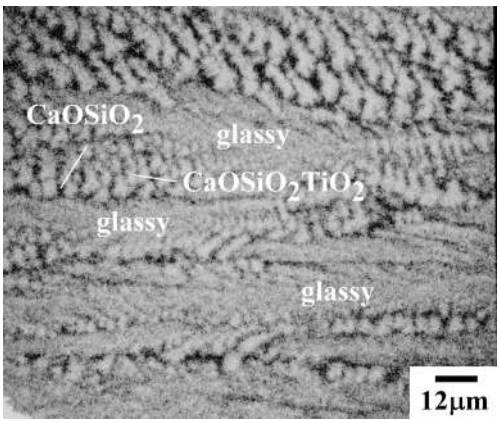

Fig. 4. Characteristic X-ray image of Ti for glass CST-B sample.

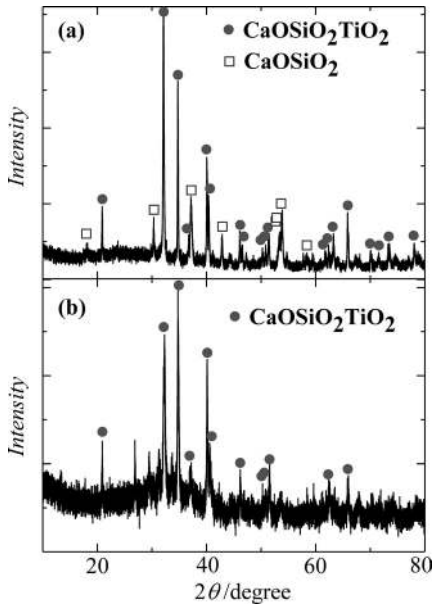

Fig. 5. X-ray diffractions of (a) glass CST-A sample and (b) glass CST-C sample.

Table 3. Results of X-ray diffraction studies and microstructure observation by EPMA.

Sample No.	cooling rate of DTA measurement /Ks^{-1}	crystal identified by XRD	crystal observed by EPMA
glass CST-A	0.173	$CaOSiO_2TiO_2$ + $CaOSiO_2$	-
glass CST-B	0.373	$CaOSiO_2TiO_2$ + $CaOSiO_2$	$CaOSiO_2TiO_2$ + $CaOSiO_2$ +glassy
glass CST-C	1.94	$CaOSiO_2TiO_2$	$CaOSiO_2TiO_2$ +glassy
glass CST-D	2.36	undetected	glassy
glass CS-A	0.173	$CaOSiO_2TiO_2$ + $CaOSiO_2$ + SiO_2	cancellate ($CaOSiO_2TiO_2$ + $CaOSiO_2$) + columnar ($CaOSiO_2TiO_2$ + $CaOSiO_2$) + SiO_2 (small grain)
glass CS-B	0.600	$CaOSiO_2TiO_2$ + $CaOSiO_2$ + SiO_2	-
glass CS-C	0.633	$CaOSiO_2TiO_2$ + $CaOSiO_2$	cancellate ($CaOSiO_2TiO_2$ + $CaOSiO_2$) + columnar ($CaOSiO_2TiO_2$ + $CaOSiO_2$) + SiO_2 (small grain) + glassy
glass CS-D	0.800	$CaOSiO_2TiO_2$ + $CaOSiO_2$ + SiO_2	-
glass CS-E	0.917	undetected	columnar ($CaOSiO_2TiO_2$ + $CaOSiO_2$) + SiO_2 (small grain) + glassy
glass CS-G	1.22	undetected	-
glass CS-J	3.35	-	columnar ($CaOSiO_2TiO_2$ + $CaOSiO_2$) + SiO_2 (small grain) + glassy

© 2006 ISIJ

is identified. In Table 3, the crystals identified by X-ray diffraction are summarized. The phases observed by EPMA can be identified by X-ray diffraction. However, no crystal phase is identified in glass CST-D sample.

3.1.2. Determination of the CCT Diagram of Glass CST

As shown in Table 3, in glass CST-D sample only glassy phase is observed by EPMA and no crystal is identified by X-ray diffraction. These results indicate that the temperature of Peak 3 in DTA data corresponds to the glass transition temperature. This is consistent with the tendency that Peak 3 is detected in samples whose cooling rate is large *e.g.* glass CST-C sample and glass CST-D sample. As shown in Fig. 4, the microstructure of glass CST-B sample includes the glassy phase, although Peak 3 is not detected in DTA data because of the small amount of the glassy phase.

Table 2 shows that glass CST-C sample has Peak 2 and Peak 3. As shown in Table 3, $CaOSiO_2TiO_2$ and glassy phases are observed by EPMA and only $CaOSiO_2TiO_2$ is identified by X-ray diffraction as shown in Fig. 5(b). Since Peak 3 corresponds to the glass transition point, it is concluded that Peak 2 is equivalent to the crystallization of $CaOSiO_2TiO_2$. The critical cooling rate for the crystallization of $CaOSiO_2TiO_2$ is defined, in this study, as 1.94 K/s due to no detection of Peak 2 in glass CST-D sample.

Figure 5(a) shows that glass CST-A sample includes both $CaOSiO_2TiO_2$ and $CaOSiO_2$. As shown in Table 2, Peak 1 and Peak 2 are detected in glass CST-A sample. Since Peak 2 is equivalent to the crystallization of $CaOSiO_2TiO_2$, it can be decided that Peak 1 represents the crystallization of $CaOSiO_2$. Although the result of DTA measurement shows that glass CST-B sample does not include Peak 1, $CaOSiO_2$ is identified by X-ray diffraction and EPMA. Due to the overlaps of Peak 1 with Peak 2, the crystallization of both $CaOSiO_2TiO_2$ and $CaOSiO_2$ occurs at the same temperature. Since in glass CST-C sample $CaOSiO_2$ is not identified by X-ray diffraction and EPMA, the critical cooling rate for the crystallization of $CaOSiO_2$ is defined as 0.373 K/s.

Figure 6(a) illustrates the CCT diagram of glass CST. Closed circles, opened triangles and opened squares represent Peak 1, Peak 2 and Peak 3, respectively. The line connected the closed circles expresses the crystallization of $CaOSiO_2$ and the line connected the opened triangles expresses the crystallization of $CaOSiO_2TiO_2$.

3.2. CCT Diagram of Glass CS

3.2.1. Identification of Phases by DTA Measurement, X-Ray Diffraction and EPMA in Glass CS

Figure 3(b) shows the DTA curve of glass CS-C sample whose cooling rate is 0.633 K/s. In glass CS-C sample, there are three exothermic peaks and these peaks are named to be Peak 1, Peak 2 and Peak 3, as shown in Fig. 3(b).

In Table 2, the crystallization temperature and the crystallization time determined by the exothermic peak positions of DTA measurement are summarized. The melting points of the samples are determined by the heating process of DTA measurement. Three kinds of peaks are observed. Peak 1 is identified in the samples whose cooling rate is relatively small. Peak 2 is identified in the samples except

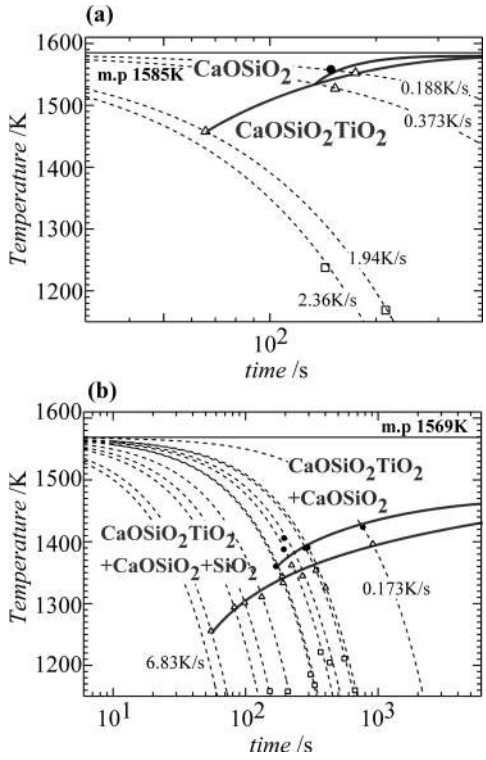

Fig. 6. CCT diagrams of (a) glass CST and (b) glass CS.

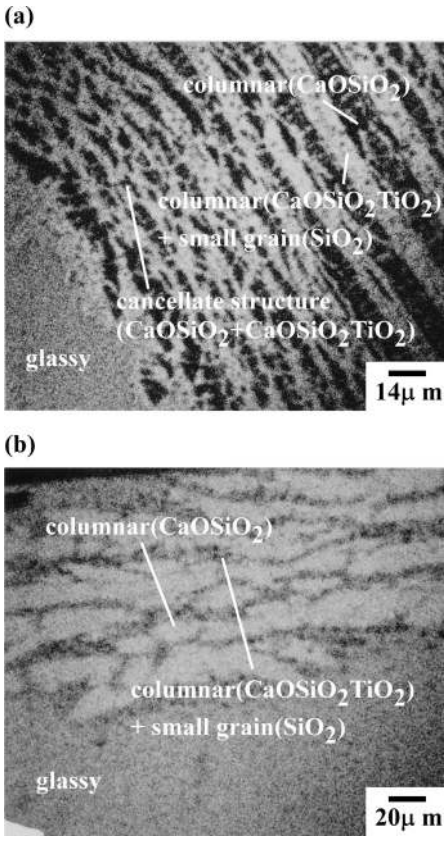

Fig. 7. Characteristic X-ray images of (a) Ti for glass CS-C sample and (b) Ca for glass CS-J sample.

glass CS-L sample. Peak 3 is identified in the samples except glass CS-A sample.

Figure 7(a) shows the characteristic X-ray image of Ti for glass CS-C sample. The middle area of Fig. 7(a) con-

© 2006 ISIJ

sists of the cancellate structure of $CaOSiO_2TiO_2$ and $CaOSiO_2$. The right upper area consists of the two columnar structures of $CaOSiO_2TiO_2$ and $CaOSiO_2$ including the small grain of SiO_2. In addition, the glassy phase is observed in the left lower area. Figure 7(b) shows the characteristic X-ray image of Ca for glass CS-J sample. In the down area of Fig. 7(b) glassy phase exists. In the upper area of Fig. 7(b) the microstructure consisting of the two columnar structures of $CaOSiO_2TiO_2$ and $CaOSiO_2$ including the small grain of SiO_2 exists. The microstructure is the same structure as the right upper area of Fig. 7(a). In Table 3, the crystals observed by EPMA observation are summarized. The microstructure consisting of the two columnar structures is observed in all samples. The cancellate structure of $CaOSiO_2TiO_2$ and $CaOSiO_2$ are observed in glass CS-A sample and glass CS-C sample. No cancellate structure is observed in glass CS-E sample and glass CS-J sample. Glassy phase is observed in glass CS-C sample, glass CS-E sample and glass CS-J sample where Peak 3 is detected.

Figures 8(a) and 8(b) show X-ray results of glass CS-A sample and glass CS-C sample, respectively. $CaOSiO_2TiO_2$, $CaOSiO_2$ and SiO_2 are identified in glass CS-A sample and only SiO_2 is not identified in glass CS-C sample due to the small intensity of the peak. In Table 3, the results of X-ray diffraction are summarized. The crystals observed by EPMA were identified by X-ray diffraction for each sample.

3.2.2. Determination of the CCT Diagram of Glass CS

Tables 2 and 3 show that the samples except glass CS-A sample include Peak 3 in DTA data and glassy phase in EPMA data. These results indicate that Peak 3 is equivalent to the glass transition point.

As shown in Fig. 7(b), the two columnar structures of $CaOSiO_2TiO_2$ and $CaOSiO_2$ including the small grain of SiO_2 and glassy phase were observed in glass CS-J sample. Peak 2 and Peak 3 were detected in DTA data of glass CS-J sample. Since the glassy phase shown in Fig. 7(b) is formed at Peak 3, it can be concluded that $CaOSiO_2TiO_2$, $CaOSiO_2$ and SiO_2 crystallize at Peak 2 simultaneously. The critical cooling rate of $CaOSiO_2TiO_2$, $CaOSiO_2$ and SiO_2 is decided as 5.70 K/s, because Peak 2 is not detected in glass CS-L sample.

Figure 7(a) shows that the microstructure of glass CS-C sample consists of the cancellate structure of $CaOSiO_2TiO_2$ and $CaOSiO_2$, the two columnar structures of $CaOSiO_2TiO_2$ and $CaOSiO_2$ including the small grain of SiO_2 and glassy phase. Glassy phase and the two columnar structures of $CaOSiO_2TiO_2$ and $CaOSiO_2$ including the small grain of SiO_2 form at Peak 3 and at Peak 2, respectively. Thus, it can be concluded that Peak 1 represents the crystallization of the cancellate structure of $CaOSiO_2TiO_2$ and $CaOSiO_2$. The critical cooling rate of the crystallization of $CaOSiO_2TiO_2$ and $CaOSiO_2$ is decided as 1.22 K/s, because Peak 1 is not detected in glass CS-H sample. Although it is expected that glass CS-F sample should include Peak 1 in DTA data, Peak 1 is not detected in glass CS-F sample by the result of DTA measurement. The intensity of Peak 1 is very small in glass CS-F sample whose cooling rate is close to the critical cooling rate. On the other hand, Peak 1 is detected in glass CS-G sample regardless of the very small intensity of Peak 1.

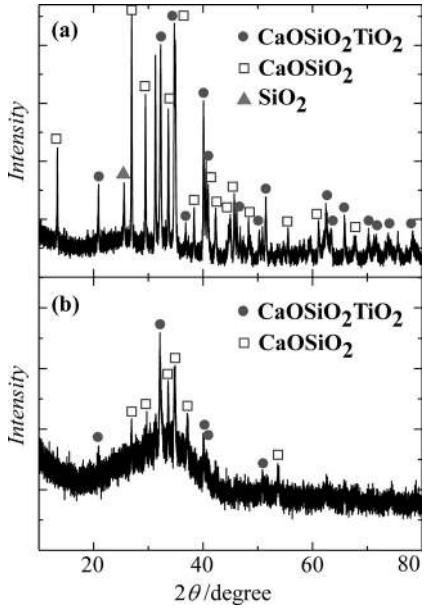

Fig. 8. X-ray diffractions of (a) glass CS-A sample and (b) glass CS-C sample.

Villegas *et al.*[25] reported that phase separation is a very common phenomenon in $CaO–SiO_2–TiO_2$ glass because TiO_2 induces liquid–liquid immiscibility. They observed the microstructure of the strong phase separation as a droplet with the size between 0.3 μm and 2 μm. As shown in Figs. 7(a) and 7(b), the small grain included in the two columnar structures, in this study, has the size of 5 μm. In addition, SiO_2 is identified by X-ray diffraction of glass CS-A sample. Thus, these results conclude that the observed small grain included in the two columnar structures is identified as not the glassy droplet of the phase separation as reported but SiO_2 crystal.

Figure 6(b) illustrates the CCT diagram of glass CS. The closed circles and the opened triangles represent the crystallization of $CaOSiO_2TiO_2$ and $CaOSiO_2$ and the crystallization of $CaOSiO_2TiO_2$, $CaOSiO_2$ and SiO_2, respectively. The opened squares express the glass transition point.

4. Discussions

4.1. Transformation of CCT Diagram into TTT Diagram

The CCT diagrams of glass CST and glass CS shown in Fig. 6 were transformed into the TTT diagrams based on the additivity rule of Scheil.[23,24] In this rule, it is assumed that the continuous cooling curve of CCT diagram consists of a lot of isothermal steps. The application of Scheil's rule provides the following Eq. (1).

$$\sum_{i=1}^{n} \frac{\Delta t_i}{\tau_i} = 1 \quad \text{.....(1)}$$

In Eq. (1), Δt_i and τ_i represent the time period for i-th isothermal step and the ideal incubation time of TTT diagram at the same temperature as that of i-th isothermal step. **Figures 9**(a) and 9(b) show the TTT diagrams of glass CST and glass CS sample, respectively. The TTT diagram of glass CST indicates that the nose incubation time of

© 2006 ISIJ

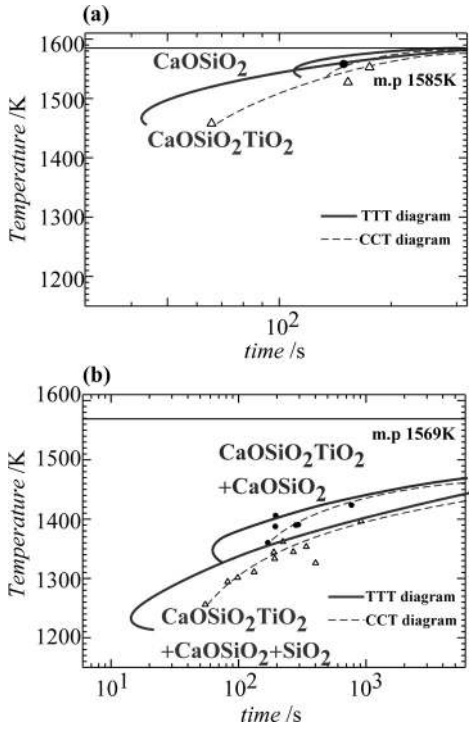

Fig. 9. TTT diagrams of (a) glass CST and (b) glass CS.

$CaOSiO_2TiO_2$ crystallizing at low temperature is far smaller than that of $CaOSiO_2$ crystallizing at high temperature. The TTT diagram of glass CS indicates that $CaOSiO_2TiO_2$ and $CaOSiO_2$ crystallize in the temperature far below the melting point. It can be stated by both TTT diagrams that $CaOSiO_2TiO_2$ has the large crystallization rate in $CaO–SiO_2–TiO_2$ slag with the basicity of around 0.8 and TiO_2 addition less than 17 mol%.

4.2. Proposal of $CaO–SiO_2–TiO_2$ Slag for Fluorine Free Mold Flux

4.2.1. Heat Transfer Control Function in $CaO–SiO_2–TiO_2$ Slag

The important roles of commercial mold fluxes are the lubrication and the heat transfer control. It has been already described in the introduction that $CaO–SiO_2–TiO_2$ slag is expected to have the lubrication function because the liquidus temperature and the viscosity are almost the same as those of $CaO–SiO_2–CaF_2$ system. Thus, in this section, the problem whether $CaO–SiO_2–TiO_2$ slag has the heat transfer control function will be discussed.

Heat transfer control is largely affected by the rapid crystallization of cuspidine in commercial mold fluxes. Thus, it is necessary that the incubation time of the crystal in $CaO–SiO_2–TiO_2$ slag is as small as that of cuspidine in commercial mold fluxes. **Figure 10** illustrates the TTT diagrams of $CaO–SiO_2–TiO_2$ slag and the commercial mold flux including CaF_2 reported by Kashiwaya *et al.*[26] in order to compare the incubation time. The TTT diagrams indicate that the incubation time of $CaOSiO_2TiO_2$ is as small as that of crystals in the commercial mold flux, cuspidine and $2CaOSiO_2$. This finding means that $CaOSiO_2TiO_2$ crystallizes rapidly in $CaO–SiO_2–TiO_2$ slag like cuspidine in the commercial mold flux. Therefore, it is considered that $CaO–SiO_2–TiO_2$ slag has the heat transfer control function.

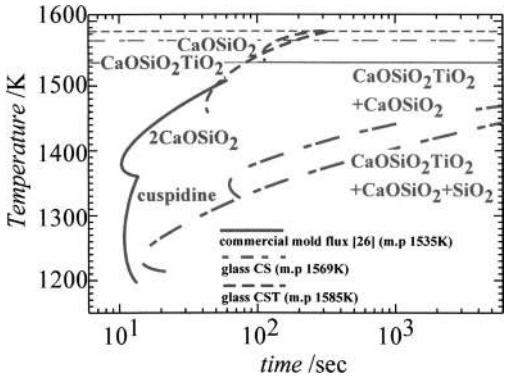

Fig. 10. TTT diagrams of the commercial mold flux, glass CS and glass CST.

4.2.2. The Substitute Crystal for Cuspidine

The basicity (CaO/SiO_2) of commercial mold fluxes is approximately 0.8 to 1.4. As shown in Fig. 2, in $CaO–SiO_2–TiO_2$ slag, the crystals which crystallize in the composition area with basicity of 0.8 to 1.4 are $CaOSiO_2TiO_2$, $CaOSiO_2$ and $CaOTiO_2$. $CaOTiO_2$ crystallizes from liquid as the following reaction (2).

$$Ca^{2+} + TiO_3^{2-} = CaOTiO_2 \quad \text{.....(2)}$$

After CaO which is a basic oxide in $CaO–SiO_2–TiO_2$ slag decomposes to Ca^{2+} and O^{2-}, Ca^{2+} modifies the silicate network. If Ca^{2+} is consumed by the reaction (2) as a result of the crystallization of $CaOTiO_2$ from liquid, the remained slag will change more acidic. Consequently, the crystallization of $CaOTiO_2$ increases the viscosity of the remained slag largely and the lubrication in $CaO–SiO_2–TiO_2$ slag is lost. Therefore, $CaOTiO_2$ is not appropriate for the substitution of cuspidine. On the other hand, since the crystallization of $CaOSiO_2TiO_2$ and $CaOSiO_2$ consume both CaO which is a basic oxide and SiO_2 which is an acidic oxide, the viscosity of the remained slag does not increase largely. As shown in Fig. 10, the incubation time of $CaOSiO_2TiO_2$ is as small as that of cuspidine, while the incubation time of $CaOSiO_2$ is far larger than that of cuspidine. These results indicate that $CaOSiO_2TiO_2$ crystal in $CaO–SiO_2–TiO_2$ slag is substituted for cuspidine in commercial mold fluxes.

4.3. Effect of the Thickness of the Crystalline Layer on Heat Transfer Control

As shown in Fig. 10, especially at high temperature, the incubation time of $CaOSiO_2TiO_2$ is far large while that of cuspidine is small. The crystalline and the liquid layers exist between the shell and the mold in commercial mold fluxes with temperature gradient from 1 800 to 500 K.[10] The difference of the incubation time at high temperature causes the problem that the thickness of the crystalline layer in $CaO–SiO_2–TiO_2$ slag is smaller than that of commercial mold fluxes. The heat transfer control is largely affected by the crystalline layer of cuspidine in commercial mold fluxes. Therefore, it is essential to discuss the effect of the thickness of the crystalline layer on the heat transfer control.

Previously, the present authors reported the effect of thermal and optical properties of mold fluxes on the heat trans-

© 2006 ISIJ

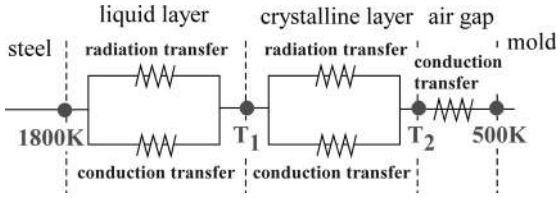

Fig. 11. Total thermal resistance of mold flux.

fer control using the heat transfer modeling.[27] In this study, the effect of the thickness of the crystalline layer on the heat transfer control is also investigated using the same modeling as follow.

The large effect of the heat transfer control means that the total thermal resistance of mold flux between the shell and the mold is large. Therefore, it is necessary to clear the relation between the thickness of the crystalline layer and the total thermal resistance of mold flux. In already reported modeling,[27] the total thermal resistance of mold flux between the shell and the mold is considered as shown in **Fig. 11**. Heat transfer through mold flux consists of both conduction and radiation transfer of the liquid and the crystalline layers. Convection transfer through mold flux can be neglected. The air gap formed by the solidification shrinkage of the crystalline layer is also taken into consideration. As shown in Fig. 11, the temperature of the boundary between the liquid and the crystalline layers corresponding to T_1, and the temperature of the boundary between the crystalline layer and the air gap corresponding to T_2 are calculated. The total thermal resistance of mold flux is calculated in the already reported way.[27] Watanabe *et al.*[11] reported that after 20 s from the casting the crystallization of cuspidine starts and the thermal resistance of mold flux increases in commercial mold fluxes. This indicates that the heat transfer control function starts to work after 20 s from the casting. Figure 10 shows that the crystallization temperature after 20 s in glass CS and the commercial mold flux are below 1 300 K and 1 450 K, respectively. Since the crystallization temperature is equivalent to the temperature T_1 shown in Fig. 11, the temperature T_1 varies from 1 300 to 1 450 K. By the heat transfer modeling,[27] the variation of the temperature T_1 corresponds to the variation of the thickness of the crystalline layer from 700 to 800 μm based on the assumption that the total thickness between the shell and the mold is 1 mm. **Figure 12** shows the relation between the thickness of the crystalline layer and the total thermal resistance of mold flux. The total thermal resistance of mold flux increases with increasing the thickness of the crystalline layer. Thus, in order to propose CaO–SiO_2–TiO_2 slag as a candidate for fluorine free mold flux, it is necessary to increase the thickness of the crystalline layer *i.e.* it is necessary to decrease the incubation time of $CaOSiO_2TiO_2$ at high temperature.

In commercial mold fluxes including CaF_2, the additional compound like Na_2O is needed for adjusting the viscosity and the liquidus temperature. It is reported that Na_2O addition to CaO–SiO_2–CaF_2 synthetic slag decreases the incubation time of cuspidine.[28] Therefore, there is a possibility that the additional compound like Na_2O also decreases the incubation time of $CaOSiO_2TiO_2$. In future, it is worth investigating the effect of Na_2O addition to CaO–SiO_2–TiO_2 slag on the crystallization behavior for the proposal of this slag as a candidate for fluorine free mold flux.

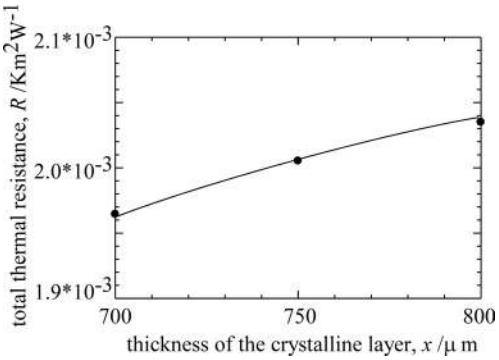

Fig. 12. Relation between the thickness of the crystalline layer and the total thermal resistance of mold flux.

5. Conclusions

Our conclusions are as follows.

(1) The TTT diagram was prepared in CaO–SiO_2–TiO_2 slag at the composition with the basicity of about 0.8 and TiO_2 addition less than 17 mol%. $CaOSiO_2TiO_2$ and $CaOSiO_2$ crystallize in this slag and the incubation time of $CaOSiO_2TiO_2$ is as small as that of cuspidine in the commercial mold flux.

(2) The crystallization of $CaOSiO_2TiO_2$ does not increase the viscosity of the remained slag and maintain the lubrication. Thus, $CaOSiO_2TiO_2$ in CaO–SiO_2–TiO_2 slag is substituted for cuspidine in commercial mold fluxes.

(3) The total thermal resistance increases with increasing the thickness of the crystalline layer. Thus, in order to propose CaO–SiO_2–TiO_2 slag as a candidate for fluorine free mold flux, it is necessary to increase the thickness of the crystalline layer *i.e.* it is necessary to decrease the incubation time of $CaOSiO_2TiO_2$ at high temperature.

REFERENCES

1) Y. Sugitani, M. Nakamura and T. Watanabe: *Tetsu-to-Hagané*, **67** (1981), 102.
2) T. J. H. Billany, A. S. Normanton and P. Grieveson: *Ironmaking Steelmaking*, **18** (1991), No. 6, 403.
3) M. Susa, K. Nagata and K. C. Mills: *Ironmaking Steelmaking*, **20** (1993), No. 5, 372.
4) M. Susa, K. C. Mills, M. J. Richardson, R. Taylor and D. Stewart: *Ironmaking Steelmaking*, **21** (1994), No. 4, 279.
5) A. Yamauchi, K. Sorimachi, T. Sakuraya and T. Fujii: *ISIJ Int.*, **33** (1993), No. 1, 140.
6) M. Kawamoto, Y. Tsukaguchi, N. Nishida, T. Kanazawa and S. Hiraki: *ISIJ Int.*, **37** (1997), No. 2, 134.
7) R. Taylor and K. C. Mills: *Ironmaking Steelmaking*, **15** (1988), No. 4, 187.
8) H. Shibata, T. Emi, Y. Waseda, K. Kondo, H. Ohta and K. Nakajima: *Tetsu-to-Hagané*, **82** (1996), No. 6, 46.
9) S. Bagha, N. C. Machingawuta and P. Grieveson: Proc. of the 3rd Int. Conf. on Molten Slag and Fluxes, The Institute of Metals, London, (1988), 235.
10) J. W. Cho, T. Emi, H. Shibata and M. Suzuki: *ISIJ Int.*, **38** (1998), No. 8, 834.
11) K. Watanabe, M. Suzuki, K. Murakami, H. Kondo, A. Miyamoto and T. Shiomi: *Tetsu-to-Hagané*, **83** (1997), No. 2, 31.
12) J. W. Cho, H. Shibata, T. Emi and M. Suzuki: *ISIJ Int.*, **38** (1998), No. 5, 440.
13) A. Yamauchi, K. Sorimachi and T. Yamauchi: *Ironmaking Steel-*

© 2006 ISIJ

making, **29** (2002), No. 3, 203.
14) H. Shibata, K. Kondo, M. Suzuki and T. Emi: *ISIJ Int.*, **36** (1996), Supplement, S179.
15) K. Tsutsumi, T. Nagasaka and M. Hino: *ISIJ Int.*, **39** (1999), No. 11, 1150.
16) T. Watanabe, H. Fukuyama and K. Nagata: *ISIJ Int.*, **42** (2002), No. 5, 489.
17) Y. Shiraishi: *J. Jpn. Inst. Met.*, **29** (1965), 614.
18) R. C. DeVries, R. Roy and E. F. Osborn: *J. Am. Ceram. Soc.*, **38** (1955), No. 5, 158.
19) H. Schench: *Arch Eisenhüttenws*, **33** (1962), 421.
20) H. Onoda, M. Terauchi and H. Nakata: KOBE Steel, *Private Communications*, (2005).
21) M. Hanao, M. Kawamoto and T. Watanabe: *ISIJ Int.*, **44** (2004), No. 5, 827.
22) P. Grieveson, S. Bagaha, N. Machingawuta, K. Liddell and K. C. Mills: *Ironmaking Steelmaking*, **15** (1988), No. 4, 181.
23) J. L. Lee, Y. T. Pan and K. C. Hsieh: *Mater. Trans.*, *JIM*, **39** (1998), No. 1, 196.
24) E. Scheil: *Arch. Eisenhüttenwes*, **8** (1935), 565.
25) M. A. Villegas, A. de Pablos and J. M. Fernandez Navarro: *Glass Technol.*, **35** (1994), No. 6, 276.
26) Y. Kashiwaya, C. E. Cicutti and Alan W. Cramb: *ISIJ Int.*, **38** (1998), No. 4, 357.
27) H. Nakada, T. Watanabe and K. Nagata: Proc.of the 3rd Int. Cong. on the Science and Technology of Steelmaking, Ronald E. Ashburn, Charlotte, North Carolina, USA, (2005), 787.
28) H. Hashimoto, T. Watanabe and K. Nagata: *CAMP-ISIJ*, **17** (2004), 849.

© 2006 ISIJ